Fabrication and performance of 3C–SiC photocathode materials for water splitting

Haojie Li [a,1], Zidong Zhou [a,1], Xiuhua Cao [a], Zhilan Du [b], Wei Yan [a], Jiawen Li [a], Altaf Mujear [a], Yinfei Shao [a], Jing Chen [a], Xuesong Wang [a], Guohua Gao [a,***], Yuxin Zhang [b,**], Yongfeng Mei [c,d,e,f], Zhihao Bao [a,*]

[a] Shanghai Key Laboratory of Special Artificial Microstructure Materials and Technology, School of Physics Science and Engineering, Tongji University, Shanghai, 200092, China
[b] College of Materials Science and Engineering, Chongqing University, Chongqing, 400044, China
[c] Yiwu Research Institute of Fudan University, Yiwu, 322000, China
[d] Department of Materials Science & State Key Laboratory of Molecular Engineering of Polymers, Fudan University, Shanghai, 200438, China
[e] Shanghai Frontiers Science Research Base of Intelligent Optoelectronics and Perception, Institute of Optoelectronics, Fudan University, Shanghai, 200438, China
[f] International Institute of Intelligent Nanorobots and Nanosystems, Fudan University, Shanghai, 200438, China

ARTICLE INFO

ABSTRACT

Since high-performance catalysts play a vital role in energy conversion efficiency during photocatalytic hydrogen evolution (PHE), they are indispensable for clean energy production and environmental sustainability. Though a lot of semiconductor materials have been developed as catalysts for PHE by water splitting, many of them (e.g., oxides, sulfides, and phosphides) suffer from low stability and unsuitable energy band structures. In contrast, the energy band structure of cubic silicon carbide (3C–SiC) ideally spans the water redox potential, and its suitable band gap (2.36 eV) can effectively utilize most of the available sunlight. Therefore, 3C–SiC exhibits unique advantages in PHE. In this review, to aid researchers in preparing an appropriate photocatalytic material for hydrogen evolution, a thorough examination of the preparation methods of 3C–SiC is offered. The modification methods of 3C–SiC and their recent advances in enhancing its efficiency of PHE are summarized. They include morphology control, heterostructure construction, doping, and loaded co-catalysts. A deep discussion of the relationship among the photocatalytic effect, its energy band structure, and modification methods of 3C–SiC is presented. Finally, the benefits and drawbacks of various modifications for PHE are emphasized, as is the outlook for future research.

1. Introduction

Since 1990, the issue of the greenhouse effect and atmospheric pollution has gotten worse and has grown to become a serious public concern. Fossil fuel is one of the main causes of greenhouse gas emissions [1]. The development of new energy sources in lieu of fossil fuels is thus viewed by some as a significant scientific and technological challenge that humanity will face in the twenty-first century [2]. Solar energy is a renewable energy source and offers a virtually unlimited supply of energy. Many researchers suggest that utilizing solar energy to make hydrogen is a practical way to capture solar energy. The combustion of hydrogen leads to the production of environmentally safe water and provides a sustainable, green fuel source. As a result, it has a great chance of replacing fossil fuels.

PHE refers to a process in which semiconductor materials capture photons to excite electrons and holes, followed by redox reactions. Since

H. Li et al.

Fujishima and Honda demonstrated in 1972 that TiO₂ photocatalyst could produce hydrogen and oxygen, numerous photocatalysts derived from semiconductors for hydrogen evolution have been thoroughly investigated [3]. Nonetheless, each known semiconductor has its own specific limitations. For instance, titanium dioxide (TiO₂), the first catalyst for photochemical hydrolysis in metal oxide semiconductors, has good chemical and thermal stability as well as non-toxicity, making it one of the most popular photocatalysts. However, its large band gap (3.2 eV) results in a restricted capture of visible light and solar power, and the pace of hydrogen evolution is constrained by the rapid conjugation of carriers produced by photons [4]. Metal sulfides that are ideal for water reduction, like CdS (Eg = 2.4 eV) and ZnS (Eg = 3.6 eV), show greater photoresponse than oxides because of their comparatively high positions of the conduction band. Yet, they suffer from low stability due to the
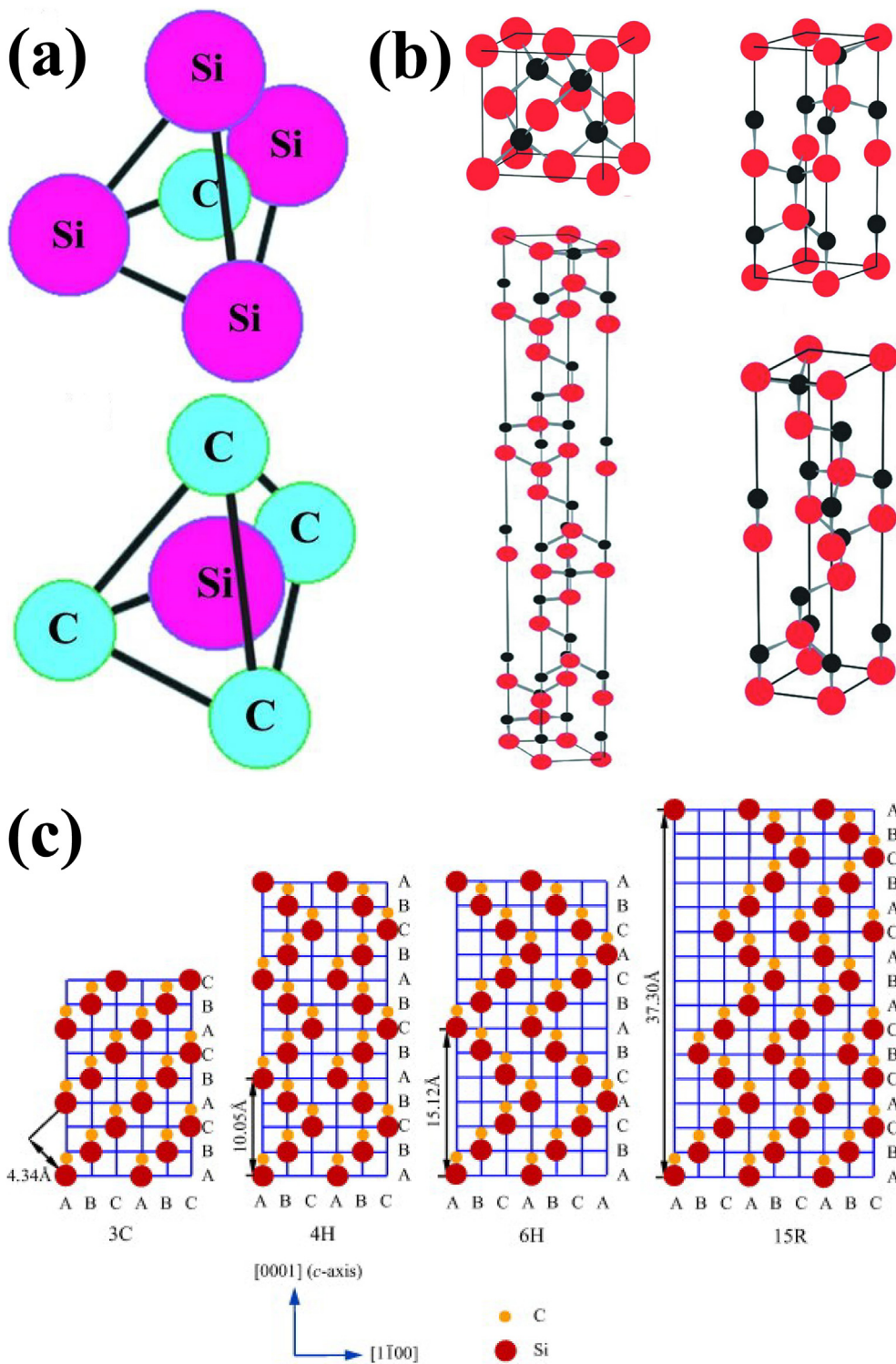
Fig. 1. **(a)** Simple tetrahedral coordination of Si and C atoms: (Top Figure) Si4C tetrahedron (C atom at the center of mass of the tetrahedron and Si atom at its vertex) and (Bottom Figure) C4Si tetrahedron (Si atom at the center of mass of the tetrahedron and C atom at its vertex) [15]. **(b)** Stacking order of 3C–SiC, 4H–SiC, 6H–SiC and 15R–SiC bilayers [15]. **(c)** Crystal structures of four SiC polytypes: 3C, 4H, 6H, and 15R (Si atoms in red and C atoms in black) [18].

photocorrosion [5]. Metal phosphides like CoP (Eg = 1.73 eV) and WP (Eg close to and superior to 1.23 eV) display excellent photocatalytic properties under dye-sensitized conditions, primarily because of their robust ability to absorb light and narrow gaps [6]. Furthermore, the band gap can be modulated by adjusting their phosphorus contents, which restrict the electron-leaving domains [7]. However, the unsuitable band positions of phosphides relative to the water redox potential hinder their application in overall solar water splitting [8]. In addition, due to their exceptional physicochemical and electrical characteristics, including their high catalytic activity, precious metals are frequently used as efficient redox co-catalysts [9]. However, photocatalysts that contain noble metals (Rh, Ag, Pt, Au, etc.), referred to as noble metal photocatalysts, have limited practical applications in aqueous decomposition because noble metal photocatalysts are more expensive and inherently rare than non-precious metal ones, which are also more efficient [10,11]. Furthermore, non-precious metal photocatalysts are also suitable for producing H_2 from wastewater since they have strong stability and do not deactivate under certain circumstances. On the contrary, Pt-based photocatalysts are susceptible to deactivation when halide ions are present [10]. To date, finding efficient and low-cost photocatalysts has been very challenging.

Silicon carbide, formed from carbon and silicon—abundant elements in the earth—is an environmentally benign semiconductor material. It has prominent durability against oxidation, strong durability against wear, exceptional endurance against shock and temperature, and a high thermal conductivity thanks to the highly covalent chemical bonding (which reaches as high as 88 %) between silicon and carbon atoms [12]. The band gap of a semiconductor material needs to be higher than 1.23 eV but less than 3.0 eV for efficient semiconductor catalytic hydrogen evolution processes powered by visible light. Additionally, the conduction band (CB) and valence band (VB) energy levels must satisfy the thermodynamic criteria for the reduction and oxidation potentials of H_2O, respectively [13]. Silicon carbide (SiC), specifically cubic silicon carbide (3C–SiC), meets these criteria with an effective band gap of 2.36 eV, enabling the absorption of visible light. Hence, when exposed to visible light, 3C–SiC acts as a viable photocatalyst [8,14].

In this review, we focus on the fundamental properties of 3C–SiC in PHE, along with its preparation methods, as well as strategies for improving PHE performance of 3C–SiC (e.g., morphology control, heterostructure construction, doping, and loaded co-catalyst.).

2. 3C–SiC properties in PHE

2.1. SiC polytypes

The fundamental building block of SiC is a main coordination tetrahedron bound by covalent bonds, such as Si_4C or C_4Si (Fig. 1(a)). Certainly, the bonds are 88 % covalent and 12 % ionic, as shown in Fig. 1(a) [15]. The distance among consecutive silicon or carbon atoms is approximately 3.08 Å, and the distance between neighboring carbon and silicon atoms is relatively short, about 1.89 Å, which results in the formation of a very strong sp^3 bond [16]. In 1947, Ramsdell introduced the most common representation of various SiC polytypes in the world [17]. Here, the Bravais lattice type (C, H, and R denote cubic, hexagonal, and rhombic, respectively) and the number of bilayers in one cycle of the lattice stack are indicated by the letters X and n, respectively. In this notation, a polytype is defined as nX [17,18]. All non-cubic structures (nH-SiC and nR-SiC) are characterized as α-SiC, while the cubic nC-SiC structure is typically known as β-SiC.

The three most prevalent silicon carbide polytypes, cubic (3C–SiC), hexagonal (4H–SiC and 6H–SiC), and rhombic (15R–SiC), are grouped in terms of atomic double stacking, as depicted in Fig. 1(b) [18], and their crystal structures are shown in Fig. 1(c) [15]. There is just one cubic form of β-SiC, 3C–SiC, which has a sphalerite-like crystal framework and an ABC … (or ACB …) stacking arrangement, as illustrated in Fig. 1(c). Similar to the diamond structure, a face-centered cubic lattice describes

β-SiC [15]. In contrast to hexagonal polytypes, the stacking order of cubic polytypes does not involve rotation, so cubic structures proceed in straight lines, and hexagonal structures proceed in zigzag patterns [16, 18].

The physical properties of SiC are strongly influenced by its different polytypes and the variation of atomic positions within them, giving rise to a diverse array of optical, electronic, and thermal attributes. Especially unlike other typical semiconductor phases, the band gap of SiC greatly changes with the polymorph, beginning at 2.4 eV for 3C–SiC and exceeding 3 eV for 4H and 6H polytypes [19]. The minimal band gap for 3C–SiC is 2.36 eV, making it an appropriate visible light-absorbing material for various applications.

2.2. Basic principle of 3C–SiC in PHE

As mentioned earlier, SiC has over 200 different polytypes, and the formation of these polytypes is related to the electronic energy band structure of silicon carbide [20]. Furthermore, the band gap of silicon carbide seems to be correlated with the relative prominence of cubic and hexagonal stacking sequences: the less cubic and more hexagonal the stacking sequence, the larger the band gap [21]. The band gaps range from 2.4 eV for 3C–SiC to 3.3 eV for 2H–SiC, with experimental values of 3.33 eV for 2H, 3.25 eV for 4H, 3.023 eV for 6H, and 2.416 eV for 3C–SiC [21,22]. It is the suitable bandgap value of 3C–SiC, which readily absorbs energy in the spectrum of visible light, that makes it more appropriate for PHE than other SiC polytypes.

The first Brillouin zone of the cubic lattice of SiC is shown in Fig. 2 (a) [22], and the energy band structure of 3C–SiC found by local density approximation (LDA) calculation is shown in Fig. 2 (b). Most SiC polytypes are indirect bandgap materials, with conduction band edges located at or near the region boundary and valence band edges located at the regional center. For example, in 3C–SiC, the conduction band edge appears to be located at point X on the region boundary. Relative to the carrier dispersion distance and space charge broadness, the optical piercing level of 3C–SiC is greater because of its modest absorption co-efficient, which is a result of its indirect bandgap nature. As a result, most of the photogenerated electron-hole pairs are distributed in the neutral region and recombined there, thus limiting photon conversion efficiency [23]. In order to ensure full absorption of sunlight, some suitable strategies, such as thickening of 3C–SiC films, are required [8].

As demonstrated by the absorption of photons, the generation, division, and migration of electron-hole pairs, as well as redox reactions during the decomposition of water, the evolution of hydrogen by photocatalysis combines photophysical, photochemical, and electrochemical processes (as depicted in Fig. 2(c)) [24]. In photocatalytic hydrolysis, the photocatalyst uses sunlight in water to directly convert H^+ to H_2, a process that is an uphill reaction with a Gibbs energy change of $\Delta G = 237$ kJ mol^{-1}. The basic requirements for a photocatalytic material are that the bandgap energy must be below 3 eV, with a theoretical minimum bandgap of 1.23 eV. The material should absorb sufficient energy photons as well as band edge potential, the bottom edge of the conduction band must be more negative than the redox potential of H^+/H_2, and the top edge of the valence band must be more positive than the redox potential of O_2/H_2O. The material should also be photocatalytically stable in electrolyte solutions in order to decompose water efficiently [25,26].

The band gap of SiC varies from 2.4 to 3.4 eV, and its energy band structure can comply with the demands of hydrogen evolution. However, the hexagonal SiC (4H- and 6H–SiC) materials from all the SiC polytypes possess wide band gaps (E_g (6H) = 3.03 eV and E_g (4H) = 3.23 eV), which means they can only absorb the ultraviolet (UV) portion of the sun spectra to break down water. Due to its comparatively small band gap of 2.36 eV, which is the closest to the presumed suitable band gap (2.03 eV) for the assumed highest level of sunlight water splitting effectiveness among all the SiC polytypes, 3C–SiC is an announcing semiconductor for photoelectrochemical (PEC) water splitting. In particular, the locations of the 3C–SiC conduction band and valence band perfectly span the redox
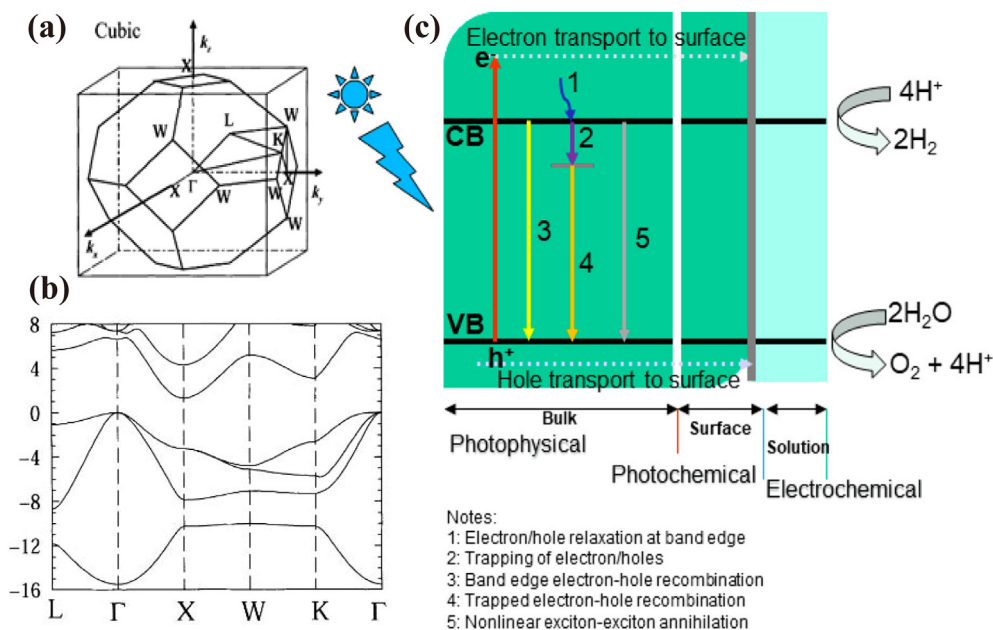
Fig. 2. **(a)** First Brillouin zone of the cubic lattice. **(b)** 3C–SiC energy band [22]. **(c)** Three key kinetic processes (photophysical, photochemical and electrochemical) involved in the overall decomposition of water [24].

potential of water. Furthermore, 3C–SiC exhibits a higher saturation drift rate and a higher carrier mobility compared to other SiC polymorphs (4H- and 6H–SiC), and these carrier transport properties play a crucial role in the absorption of light [27]. Moreover, 3C–SiC has a higher efficiency for solar PHE compared to other SiC polytypes. Therefore, we consider 3C–SiC to be the most promising candidate among all SiC polytypes for PHE [28].

Under light irradiation, 3C–SiC semiconductors absorb photons of a certain wavelength according to their intrinsic band gap. Incident photons lift electrons from the VB to the CB, leaving holes in the VB if their energy is comparable to or larger than the band gap energy of the 3C–SiC material. Hole-electron pairs are produced as a result of photon absorption. The stimulated electrons in the CB may recombine with holes that are present after radiatively or non-radiatively returning to the VB to preserve equilibrium. The independent electron-hole pairs are removed during the recombination. This is an unavoidable photophysical process that is essentially responsible for the poor quantum efficiency of the photocatalysts, regardless of the type of semiconductor used as a photocatalyst [29,30].

The reduction and oxidation procedures are sped up by transferring the uncompounded photogenerated electrons and holes to the 3C–SiC surface reaction sites. Therefore, the arrangement of the crystals, crystallization, and SiC particle dimension have a considerable impact on the division and transfer of the photogenerated pairs of electrons and holes. The crystallinity of the catalyst should be as high as possible, while the number of defects should be as low as possible for optimal charge migration. These defects serve as sites for photogenerated electron and hole capture and recombination, which lowers the photocatalytic activity [25]. When the edge of the CB is more negative (below 0 V) than the reduction potential of the adsorbed material, photogenerated electrons in the CB promote the reduction reaction and reduce H^+ in water to H_2. When the VB edge is more positive than the oxidation potential (above 1.23 V) of the adsorbed material, the holes act as an oxidant and oxidize H_2O to O_2. The surface area of photocatalyst and current condition are crucial in this stage for the accomplishment of total water splitting. The photocatalyst surface must have active sites in order for photogenerated electrons and holes to be able to breakdown water into H_2 and O_2, even if their potentials are thermodynamically sufficient to do so. At the same time, the reverse reaction of the released H_2 and O_2 to form water is

easily carried out because it is a downhill reaction. Therefore, some co-catalysts, such as Pt and Pd, are usually added to introduce the active sites for H_2 precipitation [25].

3. Preparation methods of 3C–SiC

Currently, the main methods for preparing SiC include carbon thermal reduction and magnesium thermal reduction, with the Acheson process serving as a pioneer for the carbothermal reduction technique. Unlike the carbon thermal reduction method, which necessitates temperatures above 1200 K [31,32], silica can be reduced by magnesium at lower temperatures (650 °C). The reduced silica replica retains the microscale morphology of the original silica, and the main reaction involves the reduction of SiO_2 by gaseous Mg, converting it into MgO and Si replica [33]. Thus, the low-temperature preparation of different forms of SiC can be achieved through the magnesium thermal reduction reaction [34,35].

In addition to carbon thermal reduction and magnesium thermal reduction, there are also several other SiC preparation processes. In this paper, we concentrate on the primary preparation procedures of β-SiC, such as laser pyrolysis/ablation, chemical vapor deposition, arc discharge, and solution methods.

3.1. Carbon thermal reduction

The conventional technique for making SiC is carbon thermal reduction. In their investigation of the impacts of carbon fiber characteristics on the yield, morphology, and structure of the resulting SiC, Vaguer et al. discovered that 3C–SiC was produced beyond 1400 °C and had a shape resembling that of fibers that had been covered with SiO_2. When using graphitized fibers, the chance of converting SiO to SiC was reduced, and they noted that SiC whiskers formed [32]. With carbon thermal reduction, Luo et al. successfully prepared SiC nanowires using bamboo charcoal as the carbon source without a metal catalyst. The produced nanowires develop along the <111> direction and feature a core-shell structure with diameters of approximately 50–200 nm and lengths of tens to hundreds of micrometers [31].

The sol-gel route, based on the thermal reduction of carbon, is a promising method for the preparation of β-SiC with a high surface area

and tuned nanostructures. Through the reduction of binary carbonaceous silicon dry gels generated from tetraethoxysilane-phenolic resin with nickel nitrate as a catalyst at 1250 °C, Guo et al. investigated the production of mesoporous SiC via the sol-gel technique. They discovered that by varying the amount of nitrate used during the sol-gel process, it was possible to regulate the precise surface area and pore size of mesoporous β-SiC [36,37]. Aerogels, which contain several open pores and a large surface region, facilitate mass transfer and rapid SiC formation during carbon thermal reduction. With this in mind, Li et al. successfully synthesized high-purity, highly crystalline β-SiC nanostructures using a novel RF/SiO₂ hybrid aerogel as a precursor [38]. The prepared SiC nanowhiskers were 50–150 nm in diameter and had a length of a couple of micrometers. Meanwhile, they also found the C/Si atomic ratio and heat treatment temperature in RF/SiO₂ hybrid aerogels greatly influenced the formation of SiC nanostructures. The interpenetrating matrix of the RF/SiO₂ hybrid aerogel acts as a propagation conduit for vapor products, increasing the effectiveness of carbon thermal reduction.

3.2. Magnesium thermal reduction

SiC nanocrystals prepared by the conventional carbon thermal reduction method require very high temperatures, increasing the industrial cost. The novel magnesium thermal reduction method for synthesizing β-SiC at a relatively low temperature (600 °C) effectively reduces these costs. In contrast to the traditional VLS process, the metal Mg acts as both a reducer and a catalyst. Moreover, the material generally retains its structural form in low-temperature environments.

Shi et al. synthesized an organized graded macroscopic mesoporous β-SiC material from SiO₂/C composite nanomaterials at temperatures as low as 600 °C. The entire reaction can be described as $SiO_2 + C + 2Mg \rightarrow SiC + 2MgO$. The two-step path of reaction was analyzed. First, the reduction of silica to silicon by magnesium thermal reduction ($SiO_2 + 2Mg \rightarrow Si + 2MgO$), with Mg acting as the reducing agent. In the following stage, the acquired silicon interacts with carbon to form crystalline SiC ($Si + C \rightarrow SiC$). Even though carbon and silicon should react above 1200 °C to form SiC, the temperature is significantly reduced due to the presence of Mg, which acts as a metal catalyst at this point [35].

In order to generate coordinated, single-crystal β-SiC nanorods and nanopins under supercritical fluid situations, Xi et al. developed Mg-catalyzed and reduction methods. This technology offers significant benefits over traditional elevated temperature techniques for producing homogenous semiconductor 1D nanostructures since it is effective and relatively gentle [34]. Zhao et al. successfully prepared mesoporous β-SiC with a high surface area by magnesium thermal reduction of mesoporous silica/carbon (SiO₂/C) composites (by infiltrating sucrose into the mesoporous channels of mesoporous silica) at 650 °C, a comparatively modest temperature. During the reduction process, the carbon skeleton in the composite allows the mesoporous structure of the template to be maintained. Similarly, magnesium acts not only as a reducing agent but also as a catalyst in the synthesis process [39]. Dasog et al. synthesized β-SiC nanomaterials by direct solid-state reaction of sol-gel-derived precursors, demonstrating that the method can maintain SiO₂ with different nanostructures (e.g., particles, rods, fibers) at 600 °C to convert it to SiC of the same structure. Instead of the formerly hypothesized catalytic reaction, Dasog proposed that SiC is, in this case, generated through the complicated reaction of Mg₂C₃ and SiO₂ [40].

3.3. Chemical vapor deposition

Chemical vapor deposition (CVD) is a promising technology characterized by simple systems, low costs, and the capability to produce high-purity, high-yield materials. CVD-grown nanoparticles are particularly well-suited for device fabrication and are commonly employed in the production of structural materials for optoelectronic devices. The CVD process can be categorized into vapor-liquid-solid (VLS) and vapor-solid (VS) mechanisms, with the former typically involving a catalyst and the latter not requiring one [18]. CVD is more efficient at synthesizing 0D and 1D nanomaterials compared to other methods.

In the realm of one-dimensional materials, ultra-long β-SiC nanowires hold significance for studying the inherent physical characteristics at the macroscopic scale and can be more readily applied to nanoelectronic devices than other materials [41]. In a conventional β-SiC nanowire preparation experiment, Choi et al. produced β-SiC nanowires with controlled growth using the CVD process and metal catalysts to regulate the diameter of SiC nanowires within the range of 20–50 nm [42]. Niu et al. synthesized high-quality β-SiC nanowires via direct thermal evaporation of ferrocene onto silicon wafers at high temperatures based on the VLS mechanism. Employing iron as a catalyst, ferrocene was pyrolyzed to carbon at high temperatures and subsequently deposited on the surface of Si wafers, forming SiC-NWs with diameters of about 20 nm, exhibiting good crystal structure, uniform size distribution, and a light oxide layer [43]. Similarly, Yang et al. and Sun et al. synthesized β-SiC nanowires based on VS and VLS mechanisms, respectively, using burst soot powder and silicon wafers as raw materials [44,45]. Without using any additional metal catalysts, Yang et al. created products with outstanding field-emitted characteristics in the diameter range of 30–100 nm and a length distribution of 0.5–1.5 μm [44]. Additionally, Sun et al. obtained a plethora of one-dimensional SiC structures with various morphologies, such as lines, hexagonal nanocones, and hexagonal columns, using Fe atoms as catalysts at different temperatures [45].

3.4. Solution method

The preparation of SiC nanomaterials via the solution method can effectively reduce the reaction temperature. This process might entail the naturally occurring reduction in chemical form of solution-phase compounds or additional procedures at relatively low temperatures [18]. The powders prepared by hydrothermal and solvothermal methods offer excellent homogeneity and a narrow particle size distribution [46].

Solvothermal synthesis offers a number of benefits, including moderate operating temperatures (below the reactants melting points), flexible reaction parameters, and mass manufacturing. The reaction takes place in a non-aqueous solution in an enclosed vessel, such as a stainless-steel reactor [18]. Chen et al. prepared highly dispersed silicon carbide powders using tetraethyl orthosilicate and phenolic resin at relatively low temperatures (1400–1600 °C) with a solvent-thermal-assisted sol-gel method [46]. The average microcrystalline size of the obtained SiC powder was 200 nm, and the high specific surface area was 149 m²/g. Hu et al. also successfully synthesized nanocrystalline β-SiC at 600 °C using metallic Na as a reducing agent, activated carbon, and silicon tetrachloride (SiCl₄) as raw materials [47]. The prepared SiC powder consisted of spherical particles with an average diameter of 25 nm.

Hydrothermal methods have great potential for synthesizing one-dimensional nanomaterials, as they are cost-effective, environmentally friendly, and allow the reduction of free energy in various equilibria. Pei et al. prepared one-dimensional multi-walled β-SiC nanotubes with a small diameter under supercritical hydrothermal and metal-free catalyst conditions by mixing SiC and SiO₂ powders with distilled water in a reactor (470 °C) at 9.5 MPa pressure [48,49]. The resulting nanotubes were several hundred nanometers, or even up to micrometers, in length.

4. Strategies for improving PHE performance of 3C–SiC

In the PHE process, three key dynamic processes are involved, namely the photophysical, photochemical, and electrochemical processes mentioned in the above section, for which specific manifestations (absorption of photons, generation, separation, and transfer of electron-hole pairs, and redox reactions during water splitting) need to be optimized to enhance the efficiency of hydrogen evolution by water splitting. Here we outline the primary the primary methods for improving PHE

performance of 3C–SiC, including morphological control, heterogeneous structure construction, doping, and loaded co-catalyst, and we discuss the reasons for the increased PHE efficiency of each method.

4.1. Morphological control

Morphological control is one of the most effective strategies for 3C–SiC to improve PHE. The control plays a broader role in the photocatalytic process of hydrogen evolution of 3C–SiC than other methods because of its plenty of morphological structure. For example, due to the light trapping effect, the nanoporous structure significantly decreases light reflection, increases the surface region that is electrochemically active, reduces the hole transport distance, and enables hole transport in multiple paths [23].

Zhao et al. prepared graded macroporous β-SiC monolithic materials consisting of nanocrystals directly by magnesium thermal reduction at 750 °C utilizing SiO_2 opal as a template and precursor (Fig. 3) [50]. The samples featured large specific surface areas and nanoporous structures, which enhanced the total quantity of sites for reaction and reduced charge transport pathways from the inner to outer layers of the materials, according to the results of N_2 adsorption/desorption studies. Excellent photoelectric transformation efficiency as well as durability were displayed by the macroporous β-SiC material.

Nanostructured materials, known for their larger surface area and increased reaction sites, include nanowires as a typical nanostructure that also promotes electron transfer. Hao et al. created an affordable blend of water glass and starch using carbon thermal reduction to produce β-SiC nanowires with a large surface area [51]. The diameters of the β-SiC nanowires, which varied between 70 and 400 nm and had lengths as long as 100 nm, as shown in the SEM image in Fig. 4(a), were

Fig. 3. Schematic diagrams of the formation of macroporous β-SiC [50].

randomly oriented in a straight pattern. The inset in Fig. 4(a) shows a typical TEM image of the nanowires, indicating a smooth surface and parallel stacking layer dislocations. These nanowires demonstrate extremely reliable and effective PHE via pure water when exposed to visible light (Fig. 4(b–c)). Additionally, the modification of β-SiC nanowire surfaces by acid oxidation renders the SiC nanowires highly hydrophilic, enhancing the binding of water molecules to the SiC surface and thereby improving photocatalytic activity. In terms of the nanowire morphology structure, by carbonizing Si nanowire arrangements with a powdered form of graphite at a relatively low temperature of 1250 °C, Liu et al. were able to create porous SiC nanowires arranged on Si substrates (Fig. 5) [52]. The SiC nanowires perform well in PEC hydrolysis thanks to their porous structure, which offers an extensive specific surface area as well as comparable size and length to pristine Si nanowires.

In comparison to other semiconductors, 3C–SiC film has the greatest conduction band region with a band gap of 2.4 eV, implying outstanding photoreduction capacity when exposed to visible light. Additionally, it has a strong electrocatalytic capability for H_2 generation, a quick charge transmission rate, and superior durability against corrosion [53]. Han et al. grew 3C–SiC crystalline films with heterogeneous epitaxy on (001) Si substrates with dense stacking along the ⟨110⟩ direction [54]. These epitaxial 3C–SiC films, compared with micro- and nanocrystalline 3C–SiC films, exhibited excellent PEC hydrogen evolution activity, faster transfer of charge kinetics, and a larger concentration of currents. Their superb PEC properties stem from low resistance, broad ultraviolet/visible (UV/Vis) absorption, and an ideal energy level, which hinders photogenerated carrier complexation and accelerates charge transport kinetics for PEC water splitting. The precise (001) orientation and higher phase purity of the epitaxial 3C–SiC films further improved the PEC performance. The H_2 evolution rates of 3C–SiC samples with different morphological controls are listed in Table 1.

4.2. Heterostructure construction

The photocatalytic activity of SiC is still only moderately active because photogenerated electrons and holes recombine quickly. To address this, constructing heterojunctions by joining two or more suitable materials with SiC provides space for the separation of photogenerated electrons and holes due to the energy band shift between the heterogeneous materials, thus avoiding recombination. This technique significantly raises the yield of hydrogen produced by SiC photocatalysis.

Graphene, a monolayer of graphite, is a material with a distinctive two-dimensional framework, excellent conductivity of electricity, exceptional electron transportation, as well as an exceedingly specific surface area. It is also inexpensive and feasible to fabricate on a huge scale [72]. These characteristics make it an ideal material for constructing heterojunction structures with SiC. Si–C bonds can form between SiC and graphene, creating heterojunction interfaces. SiC and graphene can quickly transport photogenerated electrons to one another thanks to chemical bonds and heterojunction surfaces, which prevent coupling with holes [65]. Zhou et al. prepared crystalline nanoparticles, ultrathin layers, or SiC films on the surface of graphene sheets (GSs) by employing a gas-solid reaction between GSs and Si powders [64]. SiC nanocrystals and graphene nanosheets work together cooperatively to increase the photocatalytic activity of SiC-GS hybrids. Yang et al. reported a method for simultaneous H_2 production and graphene oxide (GO) reduction on graphene oxide (GO)/SiC composites using KI as a sacrificial reagent for irradiation under visible light [73]. The reduced GO sheets can be used as electron collectors and transporters to effectively separate photogenerated electron-hole pairs. The photocatalytic mechanism is shown in Fig. 6 (a).

Another classic two-dimensional (2D) stratified photocatalyst possessing a good band gap (2.7 eV) and significant photocatalytic activity in the visible wavelengths is graphitic carbon nitride (g-C_3N_4), a metal-free semiconductor. It has become a promising photocatalyst due to its non-toxicity, high quantum yield, excellent chemical stability, and PEC
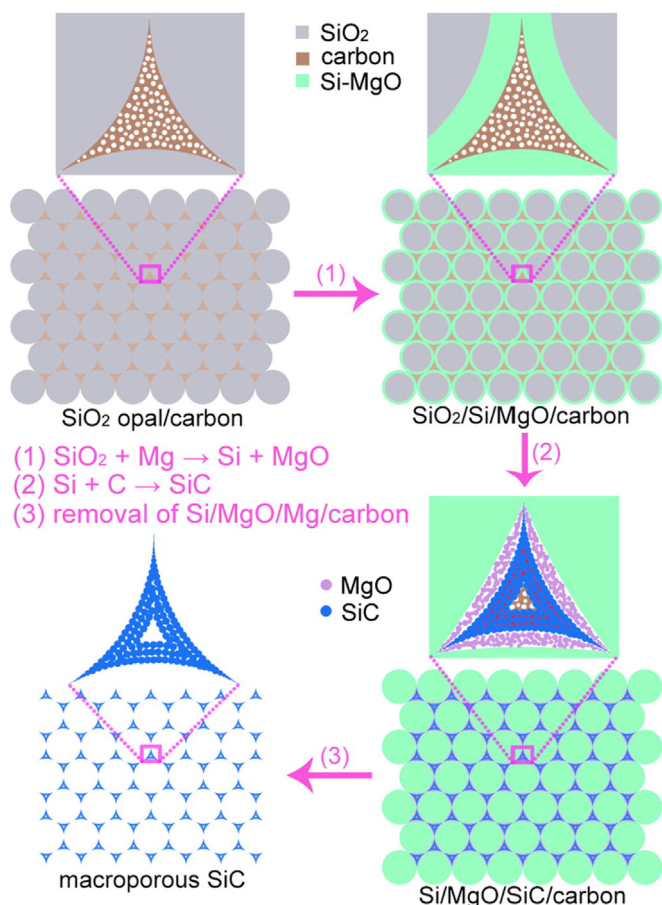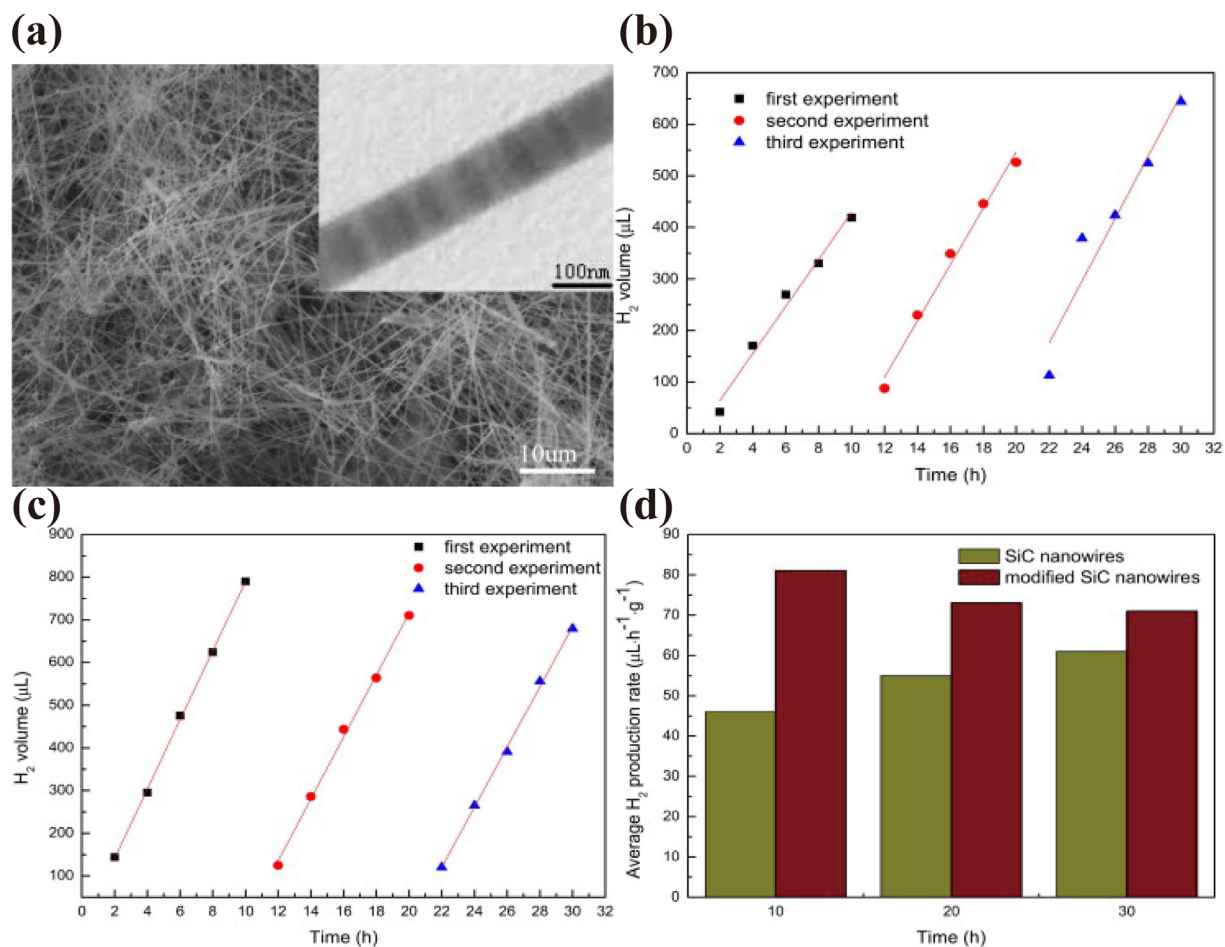
Fig. 4. (a) SEM and TEM (inset) images of the SiC nanowires. H_2 evolution of the unmodified **(b)** and modified **(c)** SiC nanowires under visible light irradiation through three non-continuous experiments. **(d)** Average H_2 production rate of the SiC nanowires and modified SiC nanowires [51].
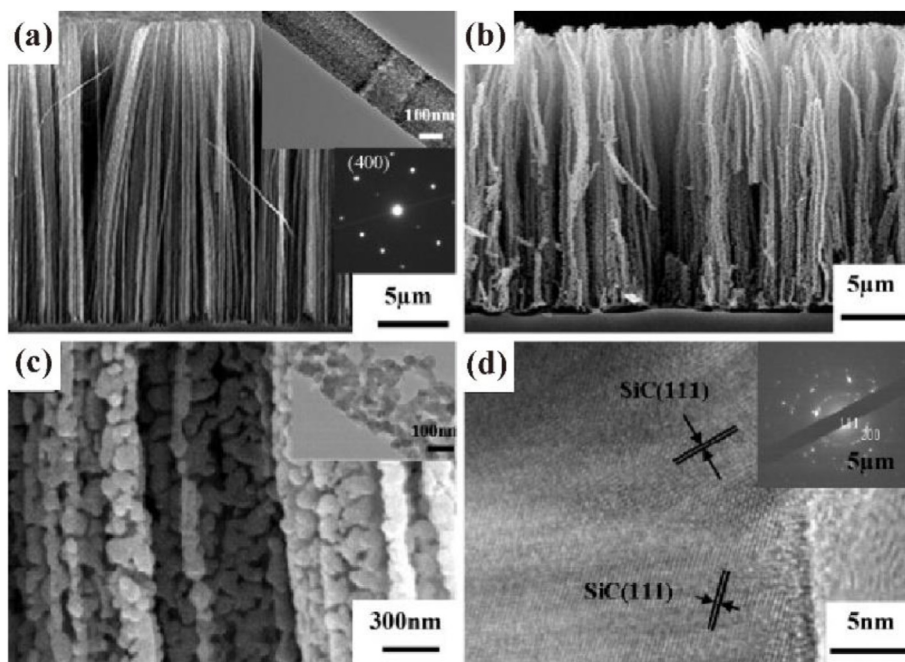

Fig. 5. Si and SiC nanowire arrays: **(a)** Cross-sectional view of SEM images of Si nanowire arrays with insets of TEM images and SAED patterns of individual Si nanowires. **(b)** Low-magnification SEM image arrays of SiC nanowires. **(c)** High-magnification SEM image arrays of SiC nanowires (insets are TEM images of individual SiC nanowires). **(d)** HRTEM images and SAED patterns (insets) of typical SiC nanowires [52].

H. Li et al.

Table 1
H$_2$ evolution on modified SiC, all unhighlighted spectral ranges are visible.

Photocatalyst	Modified mthods	H$_2$ evolution rates (μmol$\cdot$g^{-1} h^{-1})	Ref.
SiC	Whiskery, worm-like and particulate SiC	2.04 (whiskery) 3.69 (worm-like) 3.75 (particulate)	[55]
SiC	SiC nanowires was modified by acid oxidation	3.62	[51]
SiC NFs-C	Mesoporous silicon carbide nanofibers with in situ embedded carbon	180.20 (simulated solar light irradiation) 31.00 (visible light irradiation)	[56]
B–SiC	B-doped 3C–SiC nanowires with a finned microstructure	108.40	[57]
Fe–SiC	Fe-doped 3C–SiC nanowires	13.90	[58]
B–SiC	B-doped 3C–SiC	7.41	[59]
SnO$_2$/SiC	SnO$_2$/SiC hollow sphere nanochains heterostructure	825.00	[60]
SnO$_2$/SiC	SnO$_2$/SiC nanowire heterostructure	274.00 (simulated solar light irradiation)	[61]
MWCNT/SiC	Multi-walled carbon nanotube/ SiC nanowire heterostructure	108.00	[62]
CNT/SiC	Carbon nanotube/SiC coaxial heterojunction nanotubes	53.50	[63]
GSs/SiC	Ultra-thin SiC layer/graphene nanosheets heterostructure	1328.40 (white light illumination) 428.50 (visible light irradiation)	[64]
Graphene/SiC	SiC particles/graphene heterostructure	3.91	[65]
SnO$_2$/SiC	Hierarchical SnO$_2$ nanosheets/ SiC nanofibers heterostructure	471.80 (solar light irradiation)	[66]
S–TiO$_2$/SiC	S^{6+}-doped TiO$_2$/SiC heterostructure	8360.00	[67]
Cr$_2$O$_3$– TiO$_2$/ SiC	Cr3$^+$-doped TiO$_2$/SiC heterostructure	133.93	[68]
Pt/SiC NWs	Platinum nanoparticle decorated SiC nanowire	204.11 (simulated solar light irradiation)	[69]
Pt/SiC/CdS	Platinum decorated SiC/CdS heterostructure	5460.00	[70]
Ni/SiC/g-C$_3$N$_4$	Ni nanoparticles decorated SiC nanofibers/g-C$_3$N$_4$ nanosheets	6183.00	[71]

properties. However, due to the fast recombination speed of photo-generated carriers, poor charge transfer efficiency, limited surfaces, and inadequate visible light usage, the PHE yield of pure g-C$_3$N$_4$ is subpar [74,75]. As a result, it is suitable to construct heterojunctions with SiC to improve the efficiency of PHE. Through a straightforward thermal and hydrothermal process, Pan et al. created innovative SiC nano-fibers/graphitic carbon nitride (g-C$_3$N$_4$) nanosheets (SiC/CNNS) embellished with nickel (Ni) nanoparticles that serve a variety of purposes. The structure of heterojunctions promotes efficient separation and transfer of electron-hole pairs, which greatly enhances H$_2$ production [71].

TiO$_2$ photocatalysts have also been proven to be extremely promising due to their wide band gap (3.2 eV), non-toxicity, chemical stability, and photoactivation in the near-UV region of the solar spectrum [76]. However, two significant drawbacks limit their application: the relatively short excitation wavelength of light and the high complexation rate of photogenerated electron-hole pairs [77]. Constructing TiO$_2$ into heter-ojunctions with other materials greatly reduces the complexation rate of photogenerated electron-hole pairs, thus significantly improving UV light utilization efficiency [78]. Consequently, much work has focused on constructing heterostructures of SiC and TiO$_2$, which can substantially enhance photocatalytic efficiency [77,79,80]. A p-n junction forms between SiC and TiO$_2$, creating an internal built-up field through the diffusion of electrons and holes at the transition between p-type SiC and n-type TiO$_2$. When UV light is used to illuminate both SiC and TiO$_2$, this built-in potential helps to separate photogenerated electron-hole pairs by pointing from the n-side to the p-side. Electrons in the SiC conduction band transfer to the TiO$_2$ conduction band via the conventional charge transfer strategy [79,81].

Among reported n-type semiconductors, tin dioxide (SnO$_2$) has a large band gap of 3.6 eV and unique properties such as excellent thermal stability, remarkable photochemical properties, alkali resistance, acid resistance, low cost, and non-toxicity. Furthermore, SnO$_2$ has a more positive conductive band edge than SiC and is a good electron acceptor, making it widely studied for constructing heterojunction structures with SiC to facilitate PHE [60,61]. The H$_2$ evolution rates of 3C–SiC samples with different heterogeneous structures are listed in Table 1.

4.3. Doping

Doping is a traditional method for improving the efficiency of PHE, and different doping materials often lead to various effects.

Boron is also one of the most commonly used elements for doping SiC to improve the efficiency of PHE. Yang et al. utilized a simple synthetic route that combined ionic doping and morphological modification to obtain B-doped 3C–SiC nanowires (NWs) with fin-banded microstructures by adjusting the temperature of the reaction and the quantity of the boron doping (Fig. 7) [57]. This substance can produce H$_2$ at a rate of up to 108.4 μmol h^{-1}, which is around 20 times faster than 3C–SiC nanowires. It indicates that the photoinduced electrons generated by B-doped 3C–SiC can be transferred from the B-doped 3C–SiC NWS to H$^+$ and produce hydrogen under visible-light irradiation, because the potential at the edge of the CB of the B-doped 3C–SiC is more negative compared to that of the typical hydrogen electrode. Moreover, B-doping extends the absorption edge of the material to the visible region (~800 nm), and the absorption intensity is enhanced. The special fin-like single-crystal nanowires and relatively fewer stacking defects enhance electron transport, and multiple light reflections within the nanowire fins and the increased area of the suspended contacts contribute to higher PHE.

The modification effect of metal element doping is also a promising approach for the development of efficient photocatalysts operating in visible light, as the modification effect can compensate for the drawbacks of pure β-SiC by broadening the spectral response range and improving the efficiency of charge separation [82]. With this in mind, Wang et al. doped Fe into SiC nanowires, resulting in a 100-fold increase in PHE activity (Fig. 8) [58]. The H$_2$ evolution rates on different doped 3C–SiC samples are listed in Table 1.

4.4. Loaded co-catalyst

Co-catalysts are classified based on material type as metallic, non-metallic, and semiconductor [10]. Furthermore, metallic co-catalysts can be classified as noble and non-precious metal catalysts according to metal cost [83].

Presently, the most widely used precious metal co-catalyst loaded on 3C–SiC is Pt. β-SiC nanowires (Pt/SiC NWs) modified with Pt nano-particles were prepared by Wang et al. using a facile hydrothermal method [69]. The hydrogen evolution reaction was carried out under simulated sunlight irradiation without any sacrificial agent, as depicted in Fig. 9. The total H$_2$ amount and the average H$_2$ release rate of Pt/SiC nanowires exhibited stronger photocatalytic activity after 5 h of irradiation compared to pure SiC nanowires. The mechanism of the hydrogen evolution reaction on the Pt/SiC photocatalyst is illustrated in Fig. 9 (d). SiC nanowires coated with Pt nanoparticles may accept photogenerated electrons and transmit them there. Due to the low Fermi energy level of Pt, Pt nanoparticles can store photogenerated electrons, reducing the recombination rate of photogenerated charges and thus accelerating H$_2$ production.

In addition to pure SiC, Pt, as a co-catalyst, can also be loaded on SiC that has been constructed as a heterojunction, forming a ternary structure. Peng et al. used a straightforward wet chemical technique to create SiC/CdS heterojunction composite materials loaded with Pt co-catalysts [70]. Fig. 10 displays the hydrogen evolution of SiC, CdS, mechanically mixed SiC/CdS, and composites over the course of 4 h. The tight touch between SiC and CdS makes it possible for holes from the superior
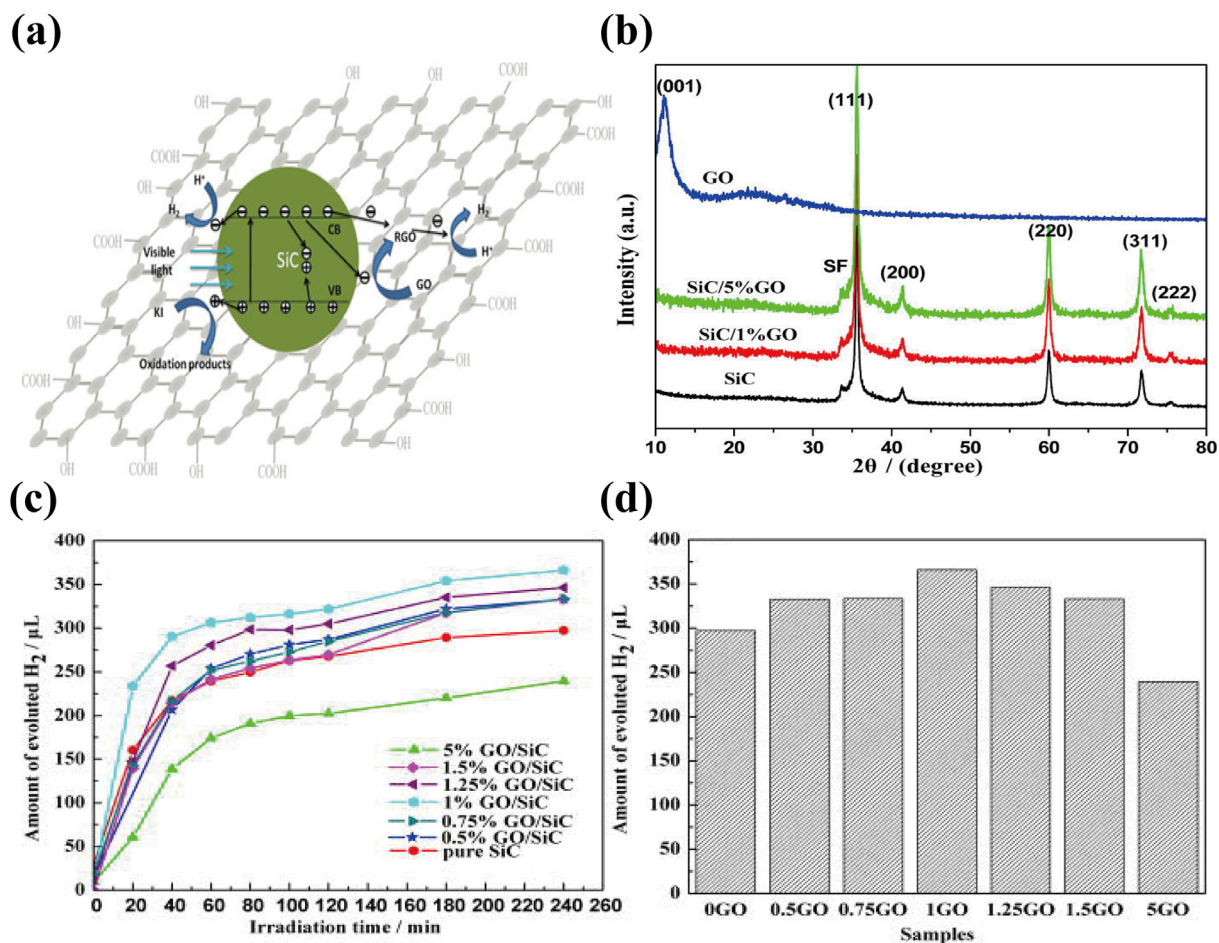
Fig. 6. (a) Schematic illustration of the charge separation and transfer in the GO/SiC system under visible light. **(b)** XRD patterns of SiC NPs, GO, 1%GO/SiC, 5%GO/SiC. Hydrogen evolution over SiC NPs in KI solution with different weight content of GO solution under visible light ($\lambda \geq 420$ nm). **(c)** Time profile, **(d)** histogram, xGO presents x% GO/SiC [73].
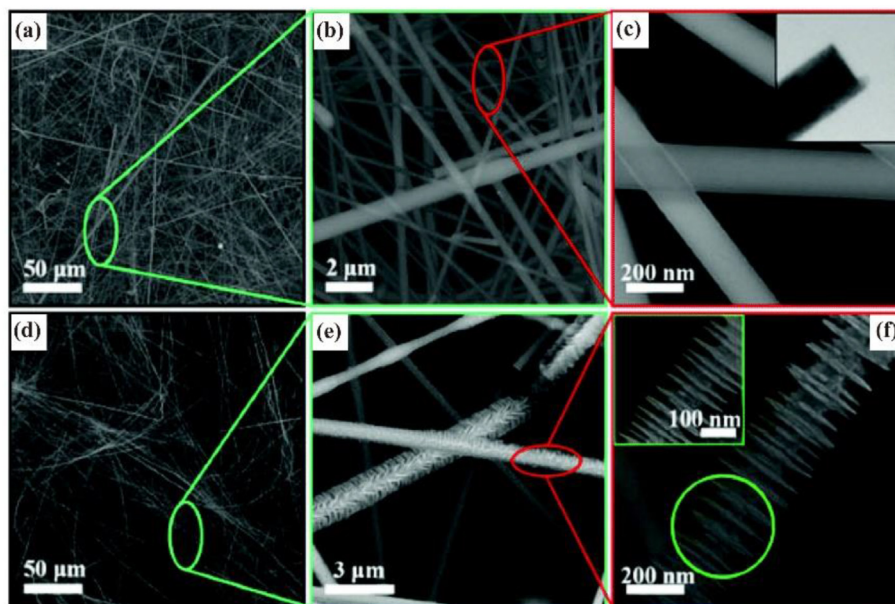

Fig. 7. SEM images of the prepared 3C–SiC **(a–c)** and B-doped 3C–SiC **(d–f)** [57].

valence band (VB) of CdS to mix with electrons from the lower conduction band (CB) of SiC at the connection point. Electrons of great energy from the higher CB of CdS finish the step of reduction on the CdS exterior to produce H_2. Additionally, the heterojunction reduces the
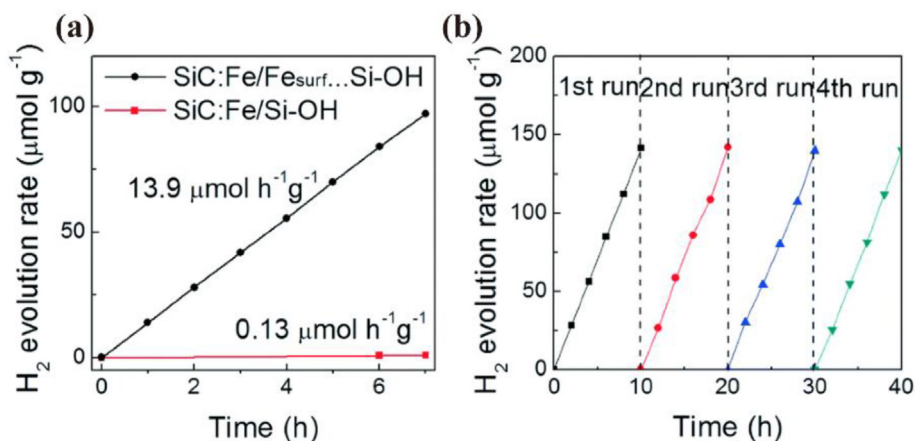
Fig. 8. H_2 production by Fe-doped SiC photocatalysts. **(a)** H_2 release rate from SiC: SiC:Fe/Fe$_{surf}$···Si–OH and surface Fe depleted photocatalysts under visible light irradiation (100 W Hg lamp used with long pass cutoff filter, $\lambda > 420$ nm). **(b)** 50 mg of SiC producing H_2 was measured repeatedly: SiC:Fe/Fe$_{surf}$···Si–OH nanowires were suspended in 100 mL of water containing only 3 mM NaI (as electron donor) at 25 °C [58].
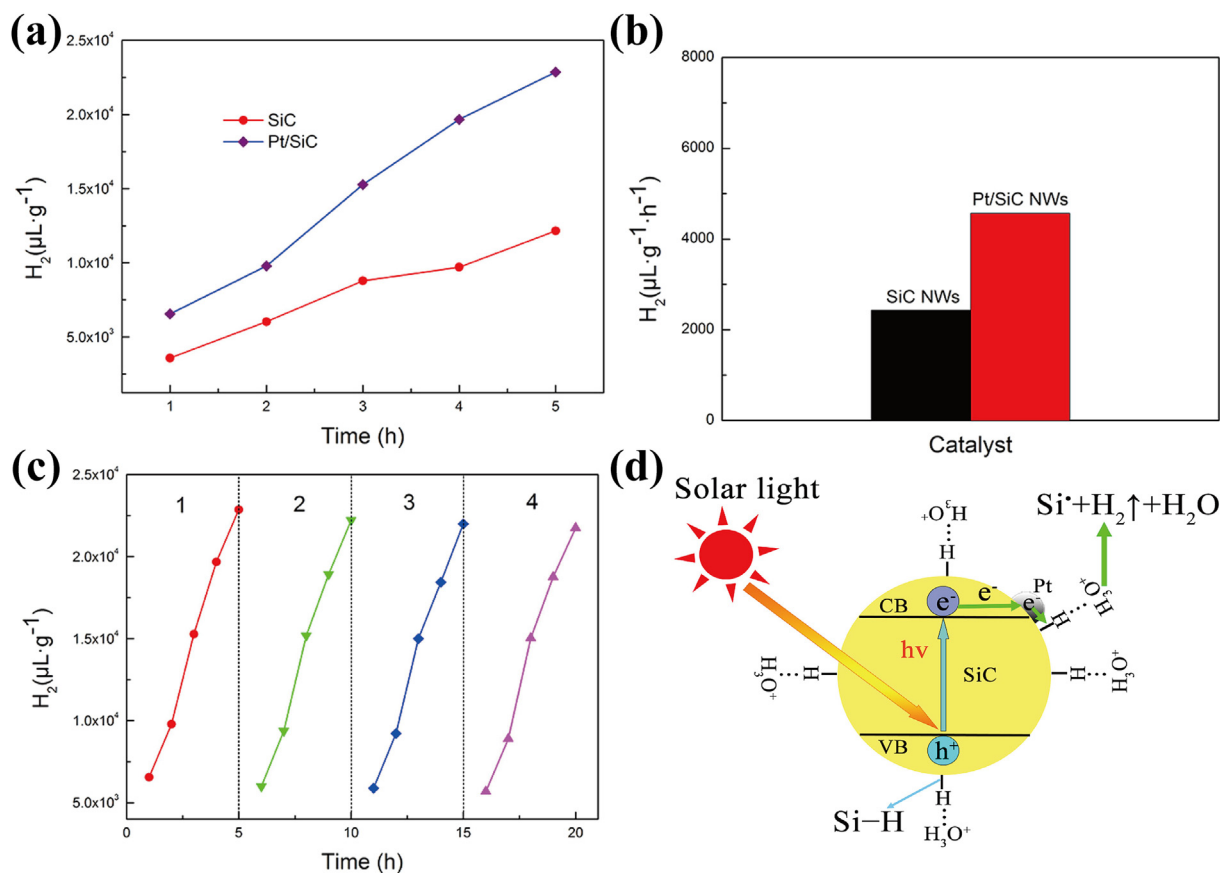

Fig. 9. H_2 release rates of Pt/SiC NWs and pure SiC NWs **(a)** and average hydrogen evolution rate **(b)**. Cycling experiments of Pt/SiC NWs on hydrolysis **(c)**. **(d)** Schematic diagram of the possible reaction mechanism of Pt/SiC photocatalyst for hydrogen evolution [69].

photocorrosion of CdS and increases the durability of the catalyst by consuming holes in its VB. The co-catalyst Pt aids in trapping photoexcited electrons to produce H_2 and lowers the PHE potential, which boosts PHE efficiency even more.

The transition metal Ni, a non-precious metal, can also be used as a co-catalyst when loaded on SiC, which has been constructed as a heterojunction. Pan et al. created unique SiC nanofibers/graphitic carbon nitride (g-C_3N_4) nanosheets (SiC/CNNS) embellished with nickel (non-precious metal) nanoparticles using a simple thermal and hydrothermal

technique [71]. The composite features a tight heterojunction interface and a substantial number of active sites, which allow to accomplish quick division of photogenerated carriers, as illustrated in Fig. 11, and this results in a maximum H_2 evolution rate (RH) of 6183 µmol g^{-1} h^{-1} for the 10 % Ni/SiC/CNNS sample. Ni acts as an electron transfer medium to construct Z-type heterojunctions, thus achieving effective bias and electron-hole pair transfer. The Ni/SiC/CNNS ternary photocatalyst enables rapid electron aggregation, efficient splitting and electron-hole pair transfer with fast reaction kinetics, and these significantly enhance H_2
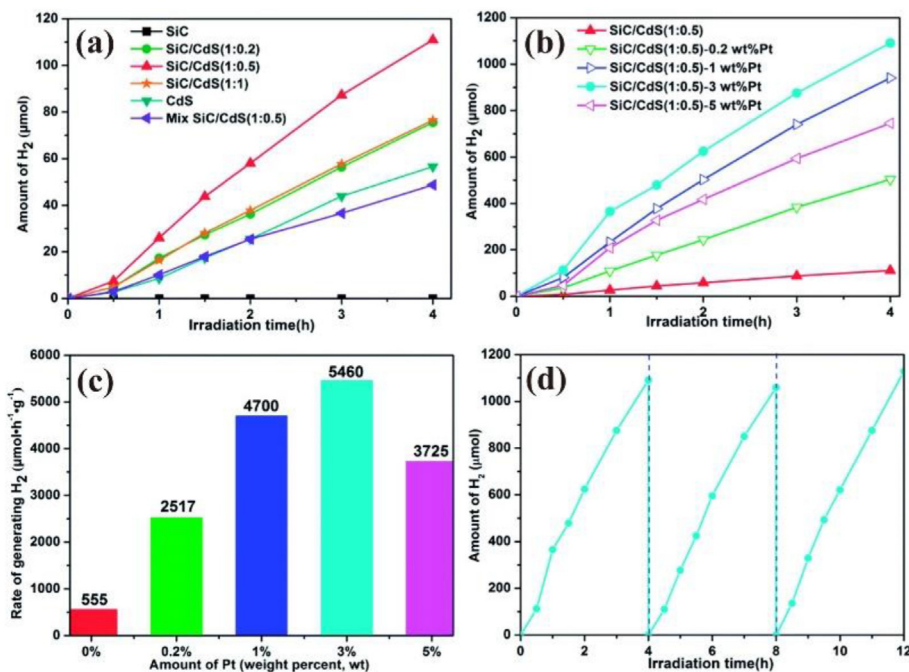
Fig. 10. PHE amounts for SiC, CdS, SiC/CdS composites and mechanically mixed SiC/CdS (1: 0.5) **(a)**. PHE amount of SiC/CdS (1: 0.5) **(b)** and hydrogen evolution rate **(c)** - x wt% Pt composite materials, x represents the percentage of mass of Pt. Recovery tests for SiC/CdS (1: 0.5)-3 wt% Pt **(d)**. Reaction conditions: 50 mg of photocatalyst was dispersed into 100 mL of deionized water containing 0.1 M $Na_2S·9H_2O$ and 0.1 M Na_2SO_3 as sacrificial reagents under visible light irradiation ($\lambda \geq$ 420 nm) [70].
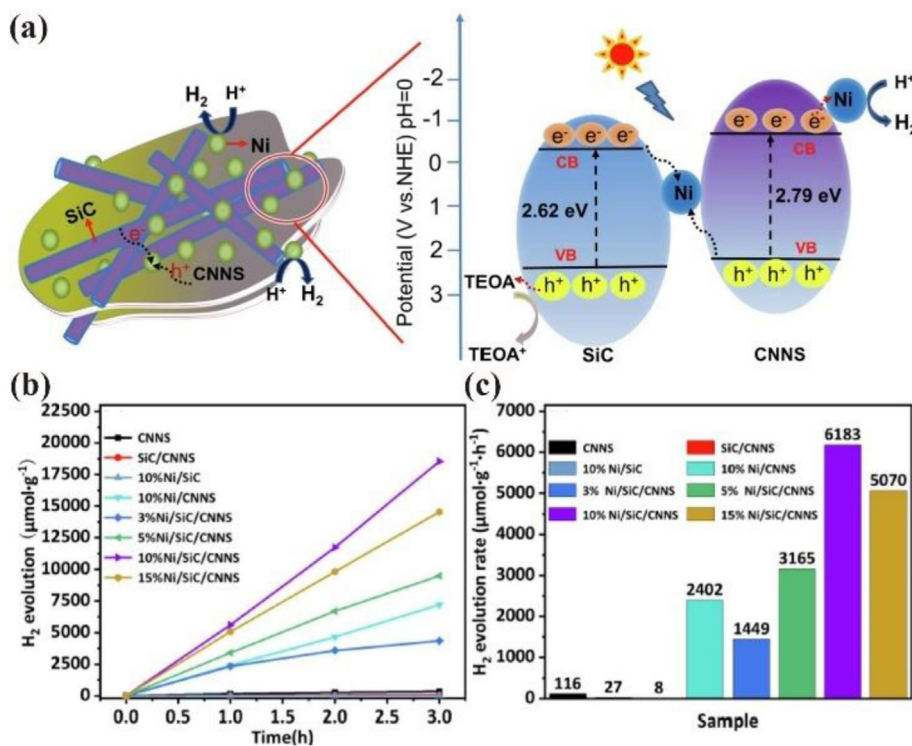

Fig. 11. (a) Schematic diagram of the photocatalytic mechanism of H_2 production on Ni/SiC/ANNS. **(b)** Amount of time variation and **(c)** H_2 release rate of samples [71].

generation due to the multiple roles of Ni as a co-catalyst and an electron transfer medium. The H_2 evolution rates on different co-catalyst-loaded 3C–SiC samples are listed in Table 1.

5. Conclusions and outlook

3C–SiC has excellent physicochemical properties as an abundant, clean, and environmentally friendly semiconductor material.

Specifically, 3C–SiC may perform PHE in harsh conditions due to its appropriate energy band structure and significant stability. However, due to the rapid recombination of photogenerated carriers, the PHE performance of 3C–SiC is seriously restricted. Therefore, a systematic review of the modification means of 3C–SiC utilized for photocatalytic water splitting hydrogen evolution is of great significance in the study of enhancing the hydrogen-evolution properties of 3C–SiC. In this paper, we systematically investigate the theoretical support of the crystalline and

energy band structures of 3C–SiC for PHE, review the important advances in the preparation of 3C–SiC in recent years, and provide technical means for the preparation of the material. Importantly, the important principles of morphology control, heterostructure construction, doping, and co-catalyst loading for the improvement of the performance of 3C–SiC are comprehensively summarized with respect to the characteristics of 3C–SiC, which provides clear guidance for the preparation of highly active 3C–SiC photocatalysts.

From the current state of the research, it can be seen that the carbon thermal reduction and magnesium thermal reduction methods are still the main methods for the preparation of 3C–SiC. The carbothermal reduction method involves a simple preparation process, low raw material costs, and wide application in the chemical and metallurgical industries. Its disadvantages, however, are the high temperature required and the high cost of time required in the experimental process. Magnesium thermal reduction is based on magnesium metal as a reducing agent and catalyst, which requires much lower temperatures than carbon thermal reduction, resulting in shorter experimental cycles, lower energy consumption, and no greenhouse gas emissions. Most importantly, the material generally does not lose its own structural morphology at low temperatures. This provides excellent experimental conditions for the preparation of structure-specific SiC materials using the template method. Chemical vapor deposition (CVD) systems are simple and inexpensive to build. Moreover, high purity and high yields of CVD-grown materials can be achieved. The preparation of SiC nanomaterials using the solution method can effectively reduce the reaction temperature. The solvothermal synthesis method has the advantages of a low operating temperature (below the melting point of the reactants), adjustable reaction parameters, and large-scale production [18]. The hydrothermal method has great potential for the synthesis of 1D nanomaterials, and it is cheap, environmentally friendly, and allows the reduction of free energy in various equilibria.

In terms of SiC modification, the morphological control is manifested in the design of nanostructures; the narrow band gap of 3C–SiC determines that it can utilize visible light, which is the most abundant in sunlight, and the nanostructures can make it possible to provide a high specific surface area, which can increase the number of reactive sites and shorten the charge-transfer paths between the interior and the surface of the material. The construction of heterojunctions solves the drawback of 3C–SiC photogenerated carriers that are prone to complexation from the energy band perspective and significantly improves the hydrogen evolution efficiency. Due to the difference in the elements, the elemental doping strategy has a larger role than the first two strategies [84,85]. However, this also means that there are no systematic theoretical explanations, so further research is required to fully understand the interactions and synergistic mechanisms between various types of elemental doping and 3C–SiC. The investigation of new affordable co-catalyst materials is crucial in the development of photocatalysts because precious metals, which are the primary source of co-catalysts, still face the issue of high cost. The study of the synergistic impacts of various strategies can also supplement the results of a single approach, which is simpler to implement and more promising for industrial promotion.

Declaration of competing interest

The authors declare that they have no known competing financial interests or personal relationships that could have appeared to influence the work reported in this paper.

Acknowledgments

References

[1] G. Bölük, M.E. Mert, Fossil & renewable energy consumption, GHGs (greenhouse gases) and economic growth: evidence from a panel of EU (European Union) countries, Energy 74 (2014) 439–446, https://doi.org/10.1016/j.energy.2014.07.008.

[2] N.S. Lewis, D.G. Nocera, Powering the planet: chemical challenges in solar energy utilization, Proc. Natl. Acad. Sci. USA 103 (2006) 15729–15735, https://doi.org/10.1073/pnas.0603395103.

[3] A. Fujishima, K. Honda, Electrochemical photolysis of water at a semiconductor electrode, Nature 238 (1972) 37–38, https://doi.org/10.1038/238037a0.

[4] M. Ge, J. Cai, J. Iocozzia, C. Cao, J. Huang, X. Zhang, et al., A review of TiO2 nanostructured catalysts for sustainable H2 generation, Int. J. Hydrogen Energy 42 (2017) 8418–8449, https://doi.org/10.1016/j.ijhydene.2016.12.052.

[5] K. Zhang, L. Guo, Metal sulphide semiconductors for photocatalytic hydrogen production, Catal. Sci. Technol. 3 (2013) 1672–1690, https://doi.org/10.1039/C3CY00018D.

[6] Y. Li, Z. Jin, H.J. Liu, H. Wang, Y. Zhang, G. Wang, Unique photocatalytic activities of transition metal phosphide for hydrogen evolution, J. Colloid Interface Sci. 541 (2019) 287–299, https://doi.org/10.1016/j.jcis.2019.01.101.

[7] Y. Shi, B. Zhang, Recent advances in transition metal phosphide nanomaterials: synthesis and applications in hydrogen evolution reaction, Chem. Soc. Rev. 45 (2016) 1529–1541, https://doi.org/10.1039/C5CS00434A.

[8] J. Jian, J. Sun, A review of recent progress on silicon carbide for photoelectrochemical water splitting, Sol. RRL 4 (7) (2020) 2000111, https://doi.org/10.1002/solr.202000111.

[9] S. Kahng, H. Yoo, J.H. Kim, Recent advances in earth-abundant photocatalyst materials for solar H2 production, Adv. Powder Technol. 31 (2020) 11–28, https://doi.org/10.1016/j.apt.2019.08.035.

[10] W.H. Zhao, Z. Chen, X. Yang, X. Qian, C. Liu, D. Zhou, et al., Recent advances in photocatalytic hydrogen evolution with high-performance catalysts without precious metals, Renewable Sustainable Energy Rev. 132 (2020) 110040, https://doi.org/10.1016/j.rser.2020.110040.

[11] J. Ran, J. Zhang, J. Yu, M. Jaroniec, S-z Qiao, Earth-abundant cocatalysts for semiconductor-based photocatalytic water splitting, Chem. Soc. Rev. 43 (2014) 7787–7812, https://doi.org/10.1039/C3CS60425J.

[12] V. Izhevskyi, L. Genova, J. Bressiani, A. Bressiani, Silicon carbide. Structure, properties and processing, Cerâmica 46 (2000) 4–13, https://doi.org/10.1590/S0366-69132000000100002.

[13] D. Jing, L. Guo, L. Zhao, X. Zhang, H. Liu, M. Li, et al., Efficient solar hydrogen production by photocatalytic water splitting: from fundamental study to pilot demonstration, Int. J. Hydrogen Energy 35 (2010) 7087–7097, https://doi.org/10.1016/j.ijhydene.2010.01.030.

[14] F. Wang, L-y Zhang, Y. Zhang, SiC nanowires synthesized by rapidly heating a mixture of SiO and arc-discharge plasma pretreated carbon black, Nanoscale Res. Lett. 4 (2008) 153–156, https://doi.org/10.1007/s11671-008-9216-3.

[15] A.L. Ortiz, F. Sanchez-Bajo, F.L. Cumbrera, F. Guiberteau, The prolific polytypism of silicon carbide, J. Appl. Crystallogr. 46 (1) (2013) 242–247, https://doi.org/10.1107/S0021889812049151.

[16] G.R. Yazdi, T. Iakimov, R. Yakimova, Epitaxial graphene on SiC: a review of growth and characterization, Crystals 6 (5) (2016) 53, https://doi.org/10.3390/cryst6050053.

[17] L.S. Ramsdell, Studies on silicon carbide, Am. Mineral. 32 (1–2) (1947) 64–82.

[18] R. Wu, K. Zhou, C.Y. Yue, J. Wei, Y. Pan, Recent progress in synthesis, properties and potential applications of SiC nanomaterials, Prog. Mater. Sci. 72 (2015) 1–60, https://doi.org/10.1016/j.pmatsci.2015.01.003.

[19] G. Tuci, Y. Liu, A. Rossin, X. Guo, C. Pham, G. Giambastiani, et al., Porous silicon carbide (SiC): a chance for improving catalysts or just another active-phase carrier? Chem. Rev. 121 (17) (2021) 10559–10665, https://doi.org/10.1021/acs.chemrev.1c00269.

[20] G. Wellenhofer, U. Rössler, Global band structure and near-band-edge states, Phys. Status Solidi 202 (1) (1997) 107–123, https://doi.org/10.1002/1521-3951(199707)202:1<107::AID-PSSB107>3.0.CO;2-9.

[21] F. Herman, R.L. Kortum, C.D. Kuglin, Energy band structure of diamond, cubic silicon carbide, silicon, and germanium, Int. J. Quant. Chem. 1 (S1) (1967) 533–566, https://doi.org/10.1002/qua.560010658.

[22] J. Dong, A.B. Chen, Fundamental properties of SiC: crystal structure, bonding energy, band structure, and lattice vibrations, in: Z.C. Feng (Ed.), SiC Power Materials: Devices and Applications, Springer Berlin Heidelberg, Berlin, Heidelberg, 2004, pp. 63–87, https://doi.org/10.1007/978-3-662-09877-6_2.

[23] J.-X. Jian, V. Jokubavicius, M. Syväjärvi, R. Yakimova, J. Sun, Nanoporous cubic silicon carbide photoanodes for enhanced solar water splitting, ACS Nano 15 (3) (2021) 5502–5512, https://doi.org/10.1021/acsnano.1c00256.

[24] M.Z. Rahman, C.B. Mullins, Understanding charge transport in carbon nitride for enhanced photocatalytic solar fuel production, Acc. Chem. Res. 52 (1) (2019) 248–257, https://doi.org/10.1021/acs.accounts.8b00542.

[25] J. Xing, W.Q. Fang, H. Zhao, H.G. Yang, Inorganic photocatalysts for overall water splitting, Chem. Asian J. 7 (4) (2012) 642–657, https://doi.org/10.1002/asia.201100772.

[26] K. Maeda, Photocatalytic water splitting using semiconductor particles: history and recent developments, J. Photochem. Photobiol. C Photochem. Rev. 12 (4) (2011) 237–268, https://doi.org/10.1016/j.jphotochemrev.2011.07.001.

[27] R.S. Pessoa, M.A. Fraga, L.V. Santos, M. Massi, H.S. Maciel, Nanostructured thin films based on TiO2 and/or SiC for use in photoelectrochemical cells: a review of the material characteristics, synthesis and recent applications, Mater. Sci. Semicond. Process. 29 (2015) 56–68, https://doi.org/10.1016/j.mssp.2014.05.053.

[28] T. Yasuda, M. Kato, M. Ichimura, T. Hatayama, Solar-to-Hydrogen conversion efficiency of water photolysis with epitaxially grown p-type SiC, Mater. Sci. Forum 740–742 (2013) 859–862. https://doi.org/10.4028/www.scientific.net/MSF.740-742.859.

[29] M.Z. Rahman, M.G. Kibria, C.B. Mullins, Metal-free photocatalysts for hydrogen evolution, Chem. Soc. Rev. 49 (6) (2020) 1887–1931, https://doi.org/10.1039/C9CS00313D.

[30] T. Li, T. Hu, L. Dai, C.M. Li, Metal-free photo- and electro-catalysts for hydrogen evolution reaction, J. Mater. Chem. A 8 (45) (2020) 23674–23698, https://doi.org/10.1039/D0TA08704A.

[31] X. Luo, W. Ma, Y. Zhou, D. Liu, B. Yang, Y. Dai, Synthesis and photoluminescence property of silicon carbide nanowires via carbothermic reduction of silica, Nanoscale Res. Lett. 5 (1) (2009) 252, https://doi.org/10.1007/s11671-009-9474-8.

[32] C. Vix-Guterl, P. Ehrburger, Effect of the properties of a carbon substrate on its reaction with silica for silicon carbide formation, Carbon 35 (10) (1997) 1587–1592, https://doi.org/10.1016/S0008-6223(97)00117-6.

[33] Z. Bao, M.R. Weatherspoon, S. Shian, Y. Cai, P.D. Graham, S.M. Allan, et al., Chemical reduction of three-dimensional silica micro-assemblies into microporous silicon replicas, Nature 446 (7132) (2007) 172–175, https://doi.org/10.1038/nature05570.

[34] G. Xi, Y. Liu, X. Liu, X. Wang, Y. Qian, Mg-catalyzed autoclave synthesis of aligned silicon carbide nanostructures, J. Phys. Chem. B 110 (29) (2006) 14172–14178, https://doi.org/10.1021/jp0617468.

[35] Y. Shi, F. Zhang, Y.-S. Hu, X. Sun, Y. Zhang, H.I. Lee, et al., Low-temperature pseudomorphic transformation of ordered hierarchical macro-mesoporous SiO2/C nanocomposite to SiC via magnesiothermic reduction, J. Am. Chem. Soc. 132 (16) (2010) 5552–5553, https://doi.org/10.1021/ja1001136.

[36] G. Xiang-Yun, J. Guo-Qiang, Pore-size control in the sol–gel synthesis of mesoporous silicon carbide, J. Mater. Sci. 40 (5) (2005) 1301–1303, https://doi.org/10.1007/s10853-005-6957-6.

[37] G.-Q. Jin, X.-Y. Guo, Synthesis and characterization of mesoporous silicon carbide, Microporous Mesoporous Mater. 60 (1) (2003) 207–212, https://doi.org/10.1016/S1387-1811(03)00378-0.

[38] X. Li, X. Chen, H. Song, Synthesis of β-SiC nanostructures via the carbothermal reduction of resorcinol–formaldehyde/SiO2 hybrid aerogels, J. Mater. Sci. 44 (17) (2009) 4661–4667, https://doi.org/10.1007/s10853-009-3714-2.

[39] B. Zhao, H. Zhang, H. Tao, Z. Tan, Z. Jiao, M. Wu, Low temperature synthesis of mesoporous silicon carbide via magnesiothermic reduction, Mater. Lett. 65 (11) (2011) 1552–1555, https://doi.org/10.1016/j.matlet.2011.02.075.

[40] M. Dasog, L.F. Smith, T.K. Purkait, J.G.C. Veinot, Low temperature synthesis of silicon carbide nanomaterials using a solid-state method, Chem. Commun. 49 (62) (2013) 7004–7006, https://doi.org/10.1039/C3CC43625J.

[41] J. Wei, K. Li, J. Chen, H. Yuan, Synthesis of centimeter-scale ultra-long SiC nanowires by simple catalyst-free chemical vapor deposition, J. Cryst. Growth 335 (1) (2011) 160–164, https://doi.org/10.1016/j.jcrysgro.2011.09.021.

[42] H.-J. Choi, H.-K. Seong, J.-C. Lee, Y.-M. Sung, Growth and modulation of silicon carbide nanowires, J. Cryst. Growth 269 (2) (2004) 472–478, https://doi.org/10.1016/j.jcrysgro.2004.05.094.

[43] J.-J. Niu, J.-N. Wang, An approach to the synthesis of silicon carbide nanowires by simple thermal evaporation of ferrocene onto silicon wafers, Eur. J. Inorg. Chem. 2007 (25) (2007) 4006–4010, https://doi.org/10.1002/ejic.200700454.

[44] G.Z. Yang, H. Cui, Y. Sun, L. Gong, J. Chen, D. Jiang, et al., Simple catalyst-free method to the synthesis of β-SiC nanowires and their field emission properties, J. Phys. Chem. C 113 (36) (2009) 15969–15973, https://doi.org/10.1021/jp906167s.

[45] Y. Sun, H. Cui, G.Z. Yang, H. Huang, D. Jiang, C.X. Wang, The synthesis and mechanism investigations of morphology controllable 1-D SiC nanostructures via a novel approach, CrystEngComm 12 (4) (2010) 1134–1138, https://doi.org/10.1039/B906171A.

[46] H. Chen, J. Jiang, H. Zhao, Synthesis of highly dispersed silicon carbide powders by a solvothermal-assisted sol–gel process, Appl. Phys. 124 (7) (2018) 470, https://doi.org/10.1007/s00339-018-1885-x.

[47] J-q Hu, Q-y Lu, K-b Tang, Y-t Qian, G-e Zhou, X-m Liu, et al., A new rapid Reduction–Carbonization route to nanocrystalline β-SiC, Chem. Mater. 11 (9) (1999) 2369–2371, https://doi.org/10.1021/cm981071o.

[48] L.Z. Pei, Y.H. Tang, Y.W. Chen, C. Guo, X.X. Li, Y. Yuan, et al., Preparation of silicon carbide nanotubes by hydrothermal method, J. Appl. Phys. 99 (11) (2006) 114306, https://doi.org/10.1063/1.2202111.

[49] L.Z. Pei, Y.H. Tang, X.Q. Zhao, Y.W. Chen, C. Guo, Formation mechanism of silicon carbide nanotubes with special morphology, J. Appl. Phys. 100 (4) (2006) 046105, https://doi.org/10.1063/1.2335606.

[50] B. Zhao, X. Guo, M. Zheng, Z. Lin, X. Guo, H. Pang, et al., Direct preparation of hierarchical macroporous β-SiC using SiO2 opal as both template and precursor and its application in water splitting, Mater. Technol. 31 (9) (2016) 526–531, https://doi.org/10.1080/10667857.2016.1182343.

[51] J.-Y. Hao, Y.-Y. Wang, X.-L. Tong, G-Q. Jin, X.-Y. Guo, Photocatalytic hydrogen production over modified SiC nanowires under visible light irradiation, Int. J. Hydrogen Energy 37 (20) (2012) 15038–15044, https://doi.org/10.1016/j.ijhydene.2012.08.021.

[52] H. Liu, G. She, L. Mu, W. Shi, Porous SiC nanowire arrays as stable photocatalyst for water splitting under UV irradiation, Mater. Res. Bull. 47 (3) (2012) 917–920, https://doi.org/10.1016/j.materresbull.2011.12.046.

[53] H. Zhuang, N. Yang, L. Zhang, R. Fuchs, X. Jiang, Electrochemical properties and applications of nanocrystalline, microcrystalline, and epitaxial cubic silicon carbide films, ACS Appl. Mater. Interfaces 7 (20) (2015) 10886–10895, https://doi.org/10.1021/acsami.5b02024.

[54] X. Han, S. Heuser, X. Tong, N. Yang, X.-Y. Guo, X. Jiang, Epitaxial cubic silicon carbide photocathodes for visible-light-driven water splitting, Chem. Eur J. 26 (16) (2020) 3586–3590, https://doi.org/10.1002/chem.201905218.

[55] J.-Y. Hao, Y.-Y. Wang, X.-L. Tong, G.-Q. Jin, X.-Y. Guo, SiC nanomaterials with different morphologies for photocatalytic hydrogen production under visible light irradiation, Catal. Today 212 (2013) 220–224, https://doi.org/10.1016/j.cattod.2012.09.023.

[56] B. Wang, Y. Wang, Y. Lei, N. Wu, Y. Gou, C. Han, et al., Mesoporous silicon carbide nanofibers with in situ embedded carbon for co-catalyst free photocatalytic hydrogen production, Nano Res. 9 (3) (2016) 886–898, https://doi.org/10.1007/s12274-015-0971-z.

[57] T. Yang, X. Chang, J. Chen, K-c Chou, X-m Hou, B-doped 3C-SiC nanowires with a finned microstructure for efficient visible light-driven photocatalytic hydrogen production, Nanoscale 7 (19) (2015) 8955–8961, https://doi.org/10.1039/C5NR01742D.

[58] Z. Wang, F.A. Armstrong, Catalysis of solar hydrogen production by iron atoms on the surface of Fe-doped silicon carbide, Catal. Sci. Technol. 6 (19) (2016) 7038–7041, https://doi.org/10.1039/C6CY01465H.

[59] L.-L. Dong, Y.-Y. Wang, X.-L. Tong, G.-Q. Jin, X.-Y. Guo, Synthesis and characterization of boron-doped SiC for visible light driven hydrogen production, Acta Phys. Chim. Sin. 30 (1) (2014) 135–140, https://doi.org/10.3866/PKU.WHXB201311052.

[60] X. Zhou, Y. Liu, X. Li, Q. Gao, X. Liu, Y. Fang, Topological morphology conversion towards SnO2/SiC hollow sphere nanochains with efficient photocatalytic hydrogen evolution, Chem. Commun. 50 (9) (2014) 1070–1073, https://doi.org/10.1039/C3CC47790H.

[61] X. Liao, J. Chen, M. Wang, Z. Liu, L. Ding, Y. Li, Enhanced photocatalytic and photoelectrochemical activities of SnO2/SiC nanowire heterostructure photocatalysts, J. Alloys Compd. 658 (2016) 642–648, https://doi.org/10.1016/j.jallcom.2015.10.269.

[62] X. Zhou, X. Li, Q. Gao, J. Yuan, J. Wen, Y. Fang, et al., Metal-free carbon nanotube–SiC nanowire heterostructures with enhanced photocatalytic H2 evolution under visible light irradiation, Catal. Sci. Technol. 5 (5) (2015) 2798–2806, https://doi.org/10.1039/C4CY01757A.

[63] X. Zhou, Q. Gao, S. Yang, Y. Fang, Carbon nanotube@ silicon carbide coaxial heterojunction nanotubes as metal-free photocatalysts for enhanced hydrogen evolution, Chin. J. Catal. 41 (1) (2020) 62–71, https://doi.org/10.1016/S1872-2067(19)63421-2.

[64] X. Zhou, Q. Gao, X. Li, Y. Liu, S. Zhang, Y. Fang, et al., Ultra-thin SiC layer covered graphene nanosheets as advanced photocatalysts for hydrogen evolution, J. Mater. Chem. A 3 (20) (2015) 10999–11005, https://doi.org/10.1039/C5TA02516H.

[65] Y. Wang, X. Guo, L. Dong, G. Jin, Y. Wang, X.-Y. Guo, Enhanced photocatalytic performance of chemically bonded SiC-graphene composites for visible-light-driven overall water splitting, Int. J. Hydrogen Energy 38 (29) (2013) 12733–12738, https://doi.org/10.1016/j.ijhydene.2013.07.062.

[66] L. Sun, B. Wang, Y. Wang, Hierarchical SnO2 nanosheets@SiC nanofibers for enhanced photocatalytic water splitting, Int. J. Appl. Ceram. Technol. 15 (1) (2018) 111–117, https://doi.org/10.1111/ijac.12792.

[67] G. Mishra, K.M. Parida, S.K. Singh, Facile fabrication of S-TiO2/β-SiC nanocomposite photocatalyst for hydrogen evolution under visible light irradiation, ACS Sustain. Chem. Eng. 3 (2) (2015) 245–253, https://doi.org/10.1021/sc500570k.

[68] Y. Zhang, Y. Xu, T. Li, Y. Wang, Preparation of ternary Cr2O3–SiC–TiO2 composites for the photocatalytic production of hydrogen, Particuology 10 (1) (2012) 46–50, https://doi.org/10.1016/j.partic.2011.08.001.

[69] M. Wang, J. Chen, X. Liao, Z. Liu, J. Zhang, L. Gao, et al., Highly efficient photocatalytic hydrogen production of platinum nanoparticle-decorated SiC nanowires under simulated sunlight irradiation, Int. J. Hydrogen Energy 39 (27) (2014) 14581–14587, https://doi.org/10.1016/j.ijhydene.2014.07.068.

[70] Y. Peng, Z. Guo, J. Yang, D. Wang, W. Yuan, Enhanced photocatalytic H2 evolution over micro-SiC by coupling with CdS under visible light irradiation, J. Mater. Chem. A 2 (18) (2014) 6296–6300, https://doi.org/10.1039/C4TA00468J.

[71] J. Pan, Y. Zhang, Y. Guan, Y. Yan, H. Tang, X. Liu, et al., Multifunctional Ni nanoparticles decorated SiC nanofibers/g-C3N4 nanosheets heterojunctions for drastically increased LED-light-driven hydrogen generation, Appl. Surf. Sci. 579 (2022) 152171, https://doi.org/10.1016/j.apsusc.2021.152171.

[72] Q. Xiang, J. Yu, M. Jaroniec, Graphene-based semiconductor photocatalysts, Chem. Soc. Rev. 41 (2) (2012) 782–796, https://doi.org/10.1039/C1CS15172J.

[73] J. Yang, X. Zeng, L. Chen, W. Yuan, Photocatalytic water splitting to hydrogen production of reduced graphene oxide/SiC under visible light, Appl. Phys. Lett. 102 (8) (2013) 083101, https://doi.org/10.1063/1.4792695.

[74] K.C. Christoforidis, Z. Syrgiannis, V. La Parola, T. Montini, C. Petit, E. Stathatos, et al., Metal-free dual-phase full organic carbon nanotubes/g-C3N4 heteroarchitectures for photocatalytic hydrogen production, Nano Energy 50 (2018) 468–478, https://doi.org/10.1016/j.nanoen.2018.05.070.

[75] H. Yu, R. Shi, Y. Zhao, T. Bian, Y. Zhao, C. Zhou, et al., Alkali-assisted synthesis of nitrogen deficient graphitic carbon nitride with tunable band structures for efficient

visible-light-driven hydrogen evolution, Adv. Mater. 29 (16) (2017) 1605148, https://doi.org/10.1002/adma.201605148.

[76] A.L. Linsebigler, G. Lu, J.T. Yates Jr., Photocatalysis on TiO_2 surfaces: principles, mechanisms, and selected results, Chem. Rev. 95 (3) (1995) 735–758, https://doi.org/10.1021/cr00035a013.

[77] T. Zou, C. Xie, Y. Liu, S. Zhang, Z. Zou, S. Zhang, Full mineralization of toluene by photocatalytic degradation with porous TiO_2/SiC nanocomposite film, J. Alloys Compd. 552 (2013) 504–510, https://doi.org/10.1016/j.jallcom.2012.11.061.

[78] K. Rajeshwar, M.E. Osugi, W. Chanmanee, C.R. Chenthamarakshan, M.V.B. Zanoni, P. Kajitvichyanukul, et al., Heterogeneous photocatalytic treatment of organic dyes in air and aqueous media, J. Photochem. Photobiol. C Photochem. Rev. 9 (4) (2008) 171–192, https://doi.org/10.1016/j.jphotochemrev.2008.09.001.

[79] D. Hao, Z. Yang, C. Jiang, J. Zhang, Photocatalytic activities of TiO_2 coated on different semiconductive SiC foam supports, J. Mater. Sci. Technol. 29 (11) (2013) 1074–1078, https://doi.org/10.1016/j.jmst.2013.08.021.

[80] D. Hao, Z. Yang, C. Jiang, J. Zhang, Synergistic photocatalytic effect of TiO_2 coatings and p-type semiconductive SiC foam supports for degradation of organic contaminant, Appl. Catal. B Environ. 144 (2014) 196–202, https://doi.org/10.1016/j.apcatb.2013.07.016.

[81] J. Yang, J. Feng, W. Li, X. Chen, X. Liu, J. Ruan, et al., A resource-utilization way of the waste printed circuit boards to prepare silicon carbide nanoparticles and their photocatalytic application, J. Hazard Mater. 373 (2019) 640–648, https://doi.org/10.1016/j.jhazmat.2019.03.115.

[82] H. Li, Y. Yan, S. Feng, Y. Zhu, Y. Chen, H. Fan, et al., Transition metal tuned semiconductor photocatalyst CuCo/β-SiC catalyze hydrolysis of ammonia borane to hydrogen evolution, Int. J. Hydrogen Energy 44 (16) (2019) 8307–8314, https://doi.org/10.1016/j.ijhydene.2019.02.034.

[83] S. Fang, Y.H. Hu, Recent progress in photocatalysts for overall water splitting, IJER 43 (3) (2019) 1082–1098, https://doi.org/10.1002/er.4259.

[84] G.-J. Lee, H.-C. Chen, J.J. Wu, (In, Cu) Co-doped ZnS nanoparticles for photoelectrochemical hydrogen production, Int. J. Hydrogen Energy 44 (1) (2019) 110–117, https://doi.org/10.1016/j.ijhydene.2018.02.112.

[85] Y. Cui, H. Wang, C. Yang, M. Li, Y. Zhao, F. Chen, Post-activation of in situ BF codoped g-C_3N_4 for enhanced photocatalytic H_2 evolution, Appl. Surf. Sci. 441 (2018) 621–630, https://doi.org/10.1016/j.apsusc.2018.02.073.